buildings

MDPI

*Article*

# Numerical Assessment on Bonded and Unbonded Prestressed Concrete Beams

**Miao Pang [1], Xing Liu [2], Yi Dong [2] and Tiejiong Lou [2,3,*]**

[1] Department of Civil Engineering, Zhejiang University, Hangzhou 310058, China
[2] School of Civil Engineering and Architecture, Wuhan University of Technology, Wuhan 430070, China
[3] Centre for Mechanical Engineering, Materials and Processes (CEMMPRE), University of Coimbra, 3030-788 Coimbra, Portugal
* Correspondence: tjlou@whut.edu.cn

**Abstract:** The tendon stress in bonded prestressed concrete (BPC) beams is section-dependent while it is member-dependent in unbonded prestressed concrete (UPC) beams, leading to marked difference between these two structural systems. However, little work has addressed the bond effect of steel tendons. This research presents comparative investigations of BPC and UPC beams with various prestress levels. A numerical model is experimentally validated. Numerical assessments are conducted for simply supported and continuous scenarios, focusing on the effects of bond condition and prestress level. The results show that BPC beams exhibit better crack pattern (i.e., smaller crack width with larger crack zone) than UPC beams. The difference in ultimate loads or deflections between BPC and UPC beams depends heavily on the prestress level (the values of UPC beams are around 64% and 94% of those of BPC beams at prestress levels of 25% and 75%, respectively). Unbonded tendons produce greater moment redistribution in continuous scenarios than bonded tendons. It is also shown that the ACI code cannot well describe the bond impact of steel tendons on moment redistribution in continuous scenarios. A modified ACI equation is proposed, which can predict accurately the moment redistribution in both BPC and UPC beams.

**Keywords:** bonded tendon; unbonded tendon; prestressed concrete; numerical modeling; beam



**Citation:** Pang, M.; Liu, X.; Dong, Y.; Lou, T. Numerical Assessment on Bonded and Unbonded Prestressed Concrete Beams. *Buildings* **2022**, *12*, 1658. https://doi.org/10.3390/buildings12101658

Academic Editors: Marco Bonopera and Kuo-Chun Chang

Received: 24 September 2022
Accepted: 7 October 2022
Published: 11 October 2022



## 1. Introduction

Prestressed concrete (PC) combines high concrete compression with strong tendon tension in an active manner, leading to substantially improved behavior of both materials. PC members offer many advantages over reinforced concrete (RC) counterparts such as higher structural stiffness, better durability, and smaller cross section for longer-span members. As a result, PC members are widespread in engineering such as medium and long-span PC bridges worldwide [1].

Both bonded and unbonded prestressing techniques are commonly used in practice. In bonded prestressed concrete (BPC) beams, the strain in tendons is compatible with the surrounding concrete, and thus the tendon stress is section-dependent. However, in unbonded prestressed concrete (UPC) beams, the tendons are free to move along the duct, and so there is no strain compatibility between the tendon and surrounding concrete. Friction losses in unbonded tendons are practically small, and the tendon strain is uniformly distributed along the tendon length. Therefore, the stresses in unbonded tendons are member-dependent. The difference in tendon stress evolutions results in marked performance discrepancy between BPC and UPC beams. For example, if tendons are made of fiber reinforced polymer (FRP), bonded tendons may be ruptured prior to concrete crushing while the use of unbonded technique can effectively alleviate the rupture failure [2]. Although numerous theoretical and experimental studies on BPC [3–7] and UPC beams [8–12] are available, little work has addressed the bond effect of steel tendons in PC beams [13]. Hussien et al. [13] conducted an experiment regarding simply supported BPC

and UPC beams made of different concrete grades. Their work showed that BPC beams exhibited much better structural performance than UPC beams in terms of the ductility, stiffness and deflection.

Moment redistribution occurs when a continuous beam enters into its inelastic range. Kodur and Campbell [14] carried out a parametric evaluation by utilizing a computer program and developed a pair of predictive equations for moment redistribution in continuous BPC beams depending upon loading type (concentrated load and uniformly distributed load). Lou et al. [15] examined the redistribution of moments in two-span BPC beams made of either normal or high-strength concrete. Their work showed that at a given neutral axis depth or tension steel strain, high-strength concrete led to lower moment redistribution than normal-strength concrete. Zhou and Zheng [16] performed an experimental investigation into moment redistribution in two-span UPC beams, and developed two formulae for redistribution quantification based on their test data. The relative stiffness was recognized as the most critical factor influencing moment redistribution in continuous RC [17] or PC beams [18]. Although extensive research on moment redistribution was presented, the bond impact of steel tendons on redistribution in continuous PC beams has not yet been addressed.

The prestress level is crucial in design of PC structures [19]. It is well known that the ultimate load of BPC beams is almost independent of the prestress level as bonded tendons usually have yielded before failure of the structure. By contrast, unbonded tendons generally have not yielded in failure [20] and, therefore, the ultimate load of UPC beams heavily depends on the prestress level. Consequently, the impact of prestress level on moment redistribution of BPC continuous beams may be different from that of UPC ones. Therefore, it is essential to identify the effect of prestress level in BPC and UPC beams.

This study aims to improve the state-of-the-art knowledge about the bond effect of steel tendons in PC beams. The structural behavior of BPC and UPC beams with various prestress levels is investigated by using an experimentally validated model. Two phases of numerical assessments are carried out. The first phase of study aims at examining the comprehensive response of simply supported PC beams such as the crack pattern, load-deformation behavior, stress/strain in reinforcement and neutral axis evolution, while the second phase of study emphasizes on moment redistribution in continuous PC beams.

## 2. Numerical Model and Its Validation

### *2.1. Numerical Procedure*

A finite element analysis (FEA) procedure for modeling of BPC and UPC beams was previously developed [21,22]. The following assumptions were adopted: plane sections remain plane after deformation (unbonded tendons are excluded because of the strain incompatibility between the tendons and surrounding concrete [23–26]); bonded reinforcements perfectly interact with the concrete; shear deformations are negligible; and friction losses in unbonded tendons are negligible.

The stress-strain responses of concrete, prestressing and nonprestressed steels are respectively shown in Figure 1a–c, in which $\sigma$ and $\varepsilon$ represent stress and strain, respectively; subscripts $c$, $p$ and $s$ are concrete, prestressing steel and nonprestressed steel, respectively; $E$ is the elastic modulus; $\varepsilon_0$, $\varepsilon_{cu}$ and $\varepsilon_{ck}$ are concrete compressive strain at peak stress, ultimate compressive strain and cracking strain, respectively; $f_{cm}$ and $f_t$ are concrete mean compressive strength and tensile strength, respectively; $f_{py}$ and $f_{pu}$ are prestressing steel yield stress and tensile strength, respectively; and $f_y$ is the nonprestressed steel yield strength. According to EC2 [27], $f_{cm} = f_{ck} + 8$, where $f_{ck}$ is the concrete characteristic cylinder compressive strength. As shown in Figure 1a, the concrete under compression exhibits elastic behavior until $0.4f_{cm}$, followed by nonlinear stress-strain behavior recommended by EC2 [27]. The tensile concrete also exhibits elastic behavior until its tensile strength, followed by linear tension-stiffening. The strain at the end of tension-stiffening is $10\varepsilon_{cr}$, where $\varepsilon_{cr} = f_t/E_c$. The stress-strain curve suggested in [28] is applied for prestressing steel,

as shown in Figure 1b. Nonprestressed steel is elastic and perfectly plastic, as shown in Figure 1c.

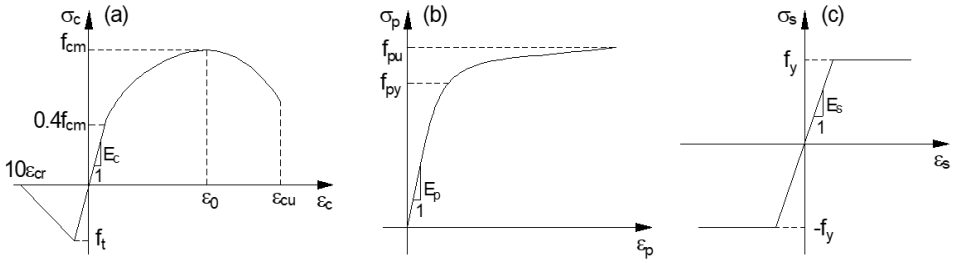


**Figure 1.** Stress-strain responses for materials. (**a**) concrete; (**b**) prestressing steel; (**c**) nonprestressed steel.

Figure 2 illustrates a beam element having nodal displacement $\boldsymbol{r}^e = \{u_i, u_j, v_i, v_j, \theta_i, \theta_j\}^T$. Assume that axial and transverse displacements are linear and cubic polynomial functions, respectively. The element tangent equilibrium equations are expressed by

$$d\boldsymbol{R}^e = \boldsymbol{K}_t^e d\boldsymbol{r}^e = (\boldsymbol{K}_o^e + \boldsymbol{K}_g^e) d\boldsymbol{r}^e \tag{1}$$

$$\boldsymbol{K}_o^e = \int_V \boldsymbol{B}^T E_t \boldsymbol{B} dV \quad \boldsymbol{K}_g^e = \int_V \sigma \boldsymbol{J}^T \boldsymbol{J} dV \tag{2}$$

$$\boldsymbol{B} = \left[ \frac{dN_1}{dx} \quad -y\frac{d^2N_2}{dx^2} \right] \boldsymbol{J} = \left[ 0 \quad 0 \quad \frac{dN_2}{dx} \right] \tag{3}$$

where $\boldsymbol{R}^e$ is element equivalent nodal loads; $\boldsymbol{r}^e$ is the element nodal displacements; $\boldsymbol{K}_t^e$ is the element tangential stiffness matrix which consists of the material stiffness matrix $\boldsymbol{K}_o^e$ and the geometrical stiffness matrix $\boldsymbol{K}_g^e$; $E_t$ is the tangential modulus; $\boldsymbol{N}_1$ and $\boldsymbol{N}_2$ are shape functions.

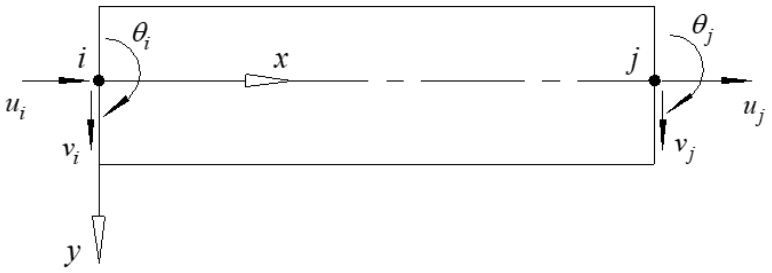


**Figure 2.** Beam element.

Note that the numerical treatments of unbonded and bonded tendons are different, i.e., unbonded tendons contribute to equivalent loads while bonded tendons contribute to stiffness matrix. Detailed numerical treatment can be seen elsewhere [21,22].

### *2.2. Model Validation*

Two PC beam specimens (A-3 and D-3) tested by Du and Tao [29] are selected for model validation. The two specimens were basically identical, except for the bond condition, i.e., Specimen A-3 was unbonded while Specimen D-3 was bonded. Both specimens were simply supported, with structure and section details illustrated in Figure 3. Material parameters are given in Table 1, where $\sigma_{p0}$ is the initial prestress; $A_p$ and $A_s$ represent the areas of prestressing and nonprestressed steels, respectively.

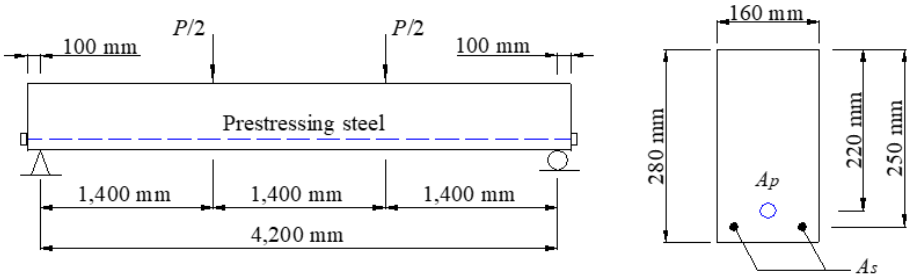


**Figure 3.** Details of PC beam specimens.

**Table 1.** Design parameters of beam specimens.

| Beam | Bond Condition | Steel Tendons | | | | | Steel Rebars | | | Concrete | | | |
|---|---|---|---|---|---|---|---|---|---|---|---|---|---|
| | | $A_p$ (mm$^2$) | $f_{py}$ (MPa) | $f_{pu}$ (MPa) | $E_p$ (GPa) | $\sigma_{p0}$ (MPa) | $A_s$ (mm$^2$) | $f_y$ (MPa) | $E_s$ (GPa) | $f_{ck}$ (MPa) | $f_t$ (MPa) | $E_c$ (GPa) | $\varepsilon_{cu}$ (%) |
| A-3 | Unbonded | 156.8 | 1465 | 1790 | 205 | 820 | 236 | 430 | 200 | 30.6 | 2.95 | 33 | 0.35 |
| D-3 | Bonded | 156.8 | 1360 | 1660 | 200 | 879 | 236 | 430 | 200 | 35.6 | 3.25 | 34 | 0.35 |

According to the FEA, both specimens fail in flexure by concrete crushing after the formation of plastic hinges over flexural span. This failure mode agrees well with the corresponding experiments. Figure 4 illustrates a comparison between numerically and experimentally obtained load-deflection curves for the two specimens. The FEA reproduces well the entire response curve, which consists of three stages, i.e., elastic stage up to cracking, cracked elastic stage until yielding (nonprestressed steel) and post-yielding stage. In addition, the FEA shows that the ultimate load of the UPC specimen (A-3) is about 10% lower than that of the BPC specimen (D-3), while the laboratory tests led to similar observations. In the following sections, a comprehensive numerical research is conducted to evaluate the bond effects in PC beams with various prestress levels.

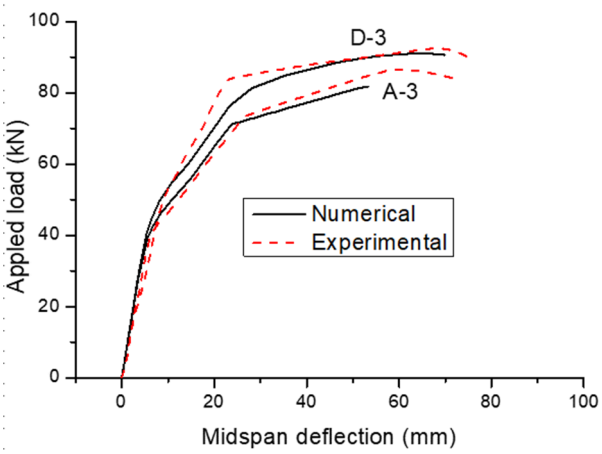


**Figure 4.** Comparison between experimentally and numerically obtained load-deflection curves.

## 3. Simply Supported Scenarios

Simply supported PC beams with horizontal steel tendons (see Figure 5) are applied for the first-phase study. Third-point loads are applied. The investigated variables are the bond condition (bonded or unbonded) and initial prestress level $\sigma_{p0}/f_{pu}$ (ratio of initial prestress to tendon tensile strength). The material parameters are as follows: $A_p$ = 900 mm$^2$, $f_{pu}$ = 1840 MPa, $f_{py}$ = 1564 MPa, $E_p$ = 200 GPa, $A_s$ = 720 mm$^2$, $f_y$ = 450 MPa, $E_s$ = 200 GPa, $f_{ck}$ = 60 MPa, $E_c$ = 39 GPa, $f_t$ = 4.4 MPa, $\varepsilon_{cu}$ = 0.003. In the analysis, the weight of the beams is converted into uniform load.

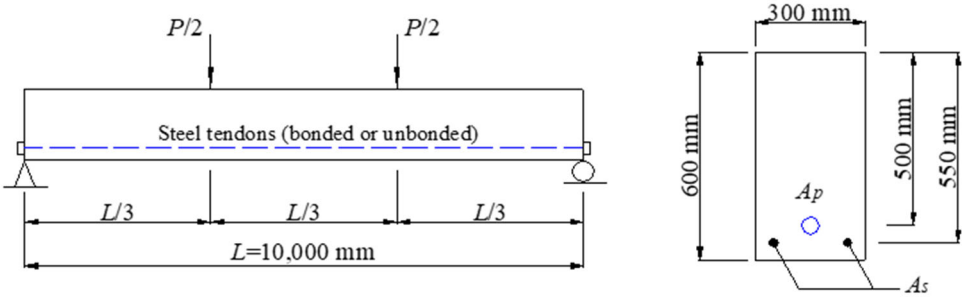


**Figure 5.** Details of simply supported PC beams for numerical investigation.

### *3.1. Crack Pattern*

Figure 6 shows the distribution of concrete tensile strains in failure in PC beams with different bond conditions and prestress levels. All failures are caused by concrete crushing at midspan. While concrete cracking is closely related to its tensile strain, the crack pattern can be deduced from the graph of Figure 6.

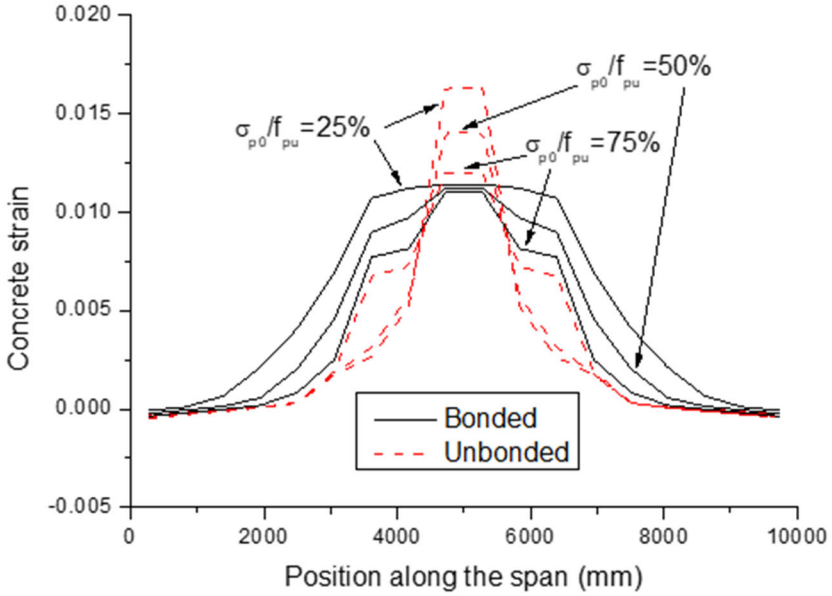


**Figure 6.** Concrete strain distribution along the span.

For BPC beams with various prestress levels, the maximum concrete tensile strains at the critical section are almost identical, indicating that the maximum crack widths in these beams are almost the same. However, the crack width over other zones for a beam with a lower prestress level is obviously larger than that for a beam with a higher prestress level. In addition, a lower prestress level leads to a larger crack zone.

For UPC beams, on the other hand, a lower prestress level mobilizes an obviously higher concrete strain at the midspan, indicating wider cracks in the critical section. Over noncritical zones, the crack widths for the 25% and 50% prestress levels are similar but considerably smaller than that for the 75% prestress level. Moreover, the beams with different prestress levels exhibit the same crack zone.

Due to the contribution of bonded tendons, BPC beams exhibit much better crack pattern than UPC beams, as expected. At a given prestress level, UPC beams have larger crack width at the midspan than BPC beams, but the difference is reduced as the prestress level increases. In the noncritical zones, the crack width for UPC beams is smaller than that for BPC beams, especially obvious at a low prestress level. The crack zone of UPC beams is smaller than that of BPC beams.

### 3.2. Moment-Curvature and Load-Deflection

Figures 7 and 8 show moment-curvature and load-deflection of BPC and UPC beams with different prestress levels, respectively. These beams, except for BPC scenarios having a 25% prestress level, exhibit three-stage behavior. The first-to-second-stage transition is attributed to concrete cracking while the following second-to-third-stage transition comes from yielding of nonprestressed steel. Each transition is featured by a marked reduction in flexural stiffness. However, the yielding of nonprestressed steel does not produce noticeable influence on the response of the BPC beam with a low prestress level of 25%. The reason could be that at yielding of nonprestressed steel, the tendons remain elastic and make greater contribution to flexural stiffness. In other words, the reduction in flexural stiffness due to nonprestressed steel yielding is compensated by increased contribution of bonded tendons.

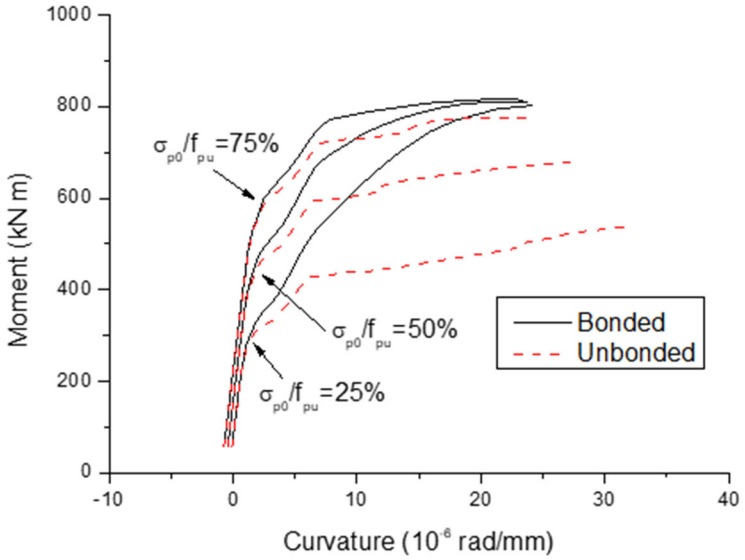


**Figure 7.** Moment-curvature curves at midspan.

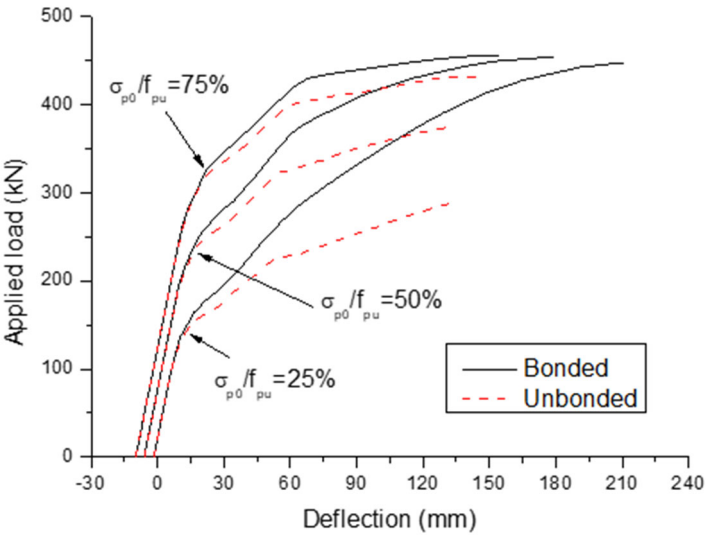


**Figure 8.** Load versus midspan deflection curves.

The prestress level has practically no influence, as expected, on the ultimate load of BPC scenarios, attributed to the fact that bonded tendons have already yielded at failure regardless of the prestress level. On the other hand, for UPC beams, the tendons have not yielded because of slowly increasing tendon stress. Therefore, a greater prestress level produces larger ultimate tendon stresses and thereby higher flexural strength and ultimate

load. The ultimate load of UPC beams is smaller than that of BPC beams, notably at a low prestress level. In this analysis, UPC beams show 35.4%, 17.4% and 5.3% lower ultimate load than BPC beams at prestress levels of 25%, 50% and 75%, respectively. Moreover, unbonded tendons lead to a greater ultimate curvature but a lower ultimate deflection compared to bonded tendons, especially at a low prestress level. In this analysis, UPC beams show 36.1%, 26.5% and 5.8% lower ultimate deflection than BPC beams at prestress levels of 25%, 50% and 75%, respectively.

### *3.3. Reinforcement Behavior*

Prestressed beams are subject to prestress losses. The tendon stress after prestress losses is called as effective prestress. The immediate prestress losses in unbonded tendons (18, 47 and 122 MPa at prestress levels of 25%, 50% and 70%, respectively) due to elastic shortening at prestress transfer are comparable to that in bonded tendons (15, 44 and 120 MPa at prestress levels of 25%, 50% and 70%, respectively). Figure 9 presents the increase in tendon stress, above the effective prestress, with the applied load. Marginal stress increment is observed at initial loading. Concrete cracking and nonprestressed steel yielding lead to much faster increase in tendon stress. After cracking, unbonded tendons show slower stress increase than bonded tendons as expected. After yielding, however, the bond condition has negligible impact on the increase rate in tendon stress. This can be explained by the fact the post-yielding moment is controlled by the prestressing tendons. Therefore, an increment in moment corresponds to certain increases in tendon stress, regardless of the bond condition.

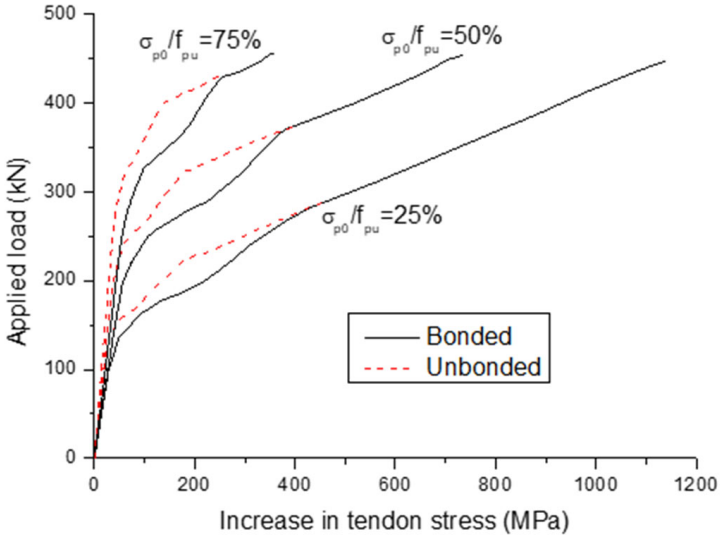


**Figure 9.** Development of tendon stress with the applied load.

At failure, unbonded tendon stress is below the yielding stress of 1564 MPa, even at a high prestress level of 75%. As a result, the tendons can be considered to be in their elastic range, which is evidenced by an approximately linear stress-deflection relationship as shown in Figure 10. In contrast, bonded tendons have yielded at ultimate, even at the prestress level of 25%. As a consequence, the stress-deflection behavior exhibits marked nonlinearity when approaching the yielding point. At the ultimate limit state, increasing prestress levels produce higher ultimate stresses in unbonded tendons, while the prestress level has negligible impacts on ultimate stresses in bonded tendons. For a given prestress level, stresses develop substantially quicker in bonded tendons than that in unbonded tendons when deflecting.

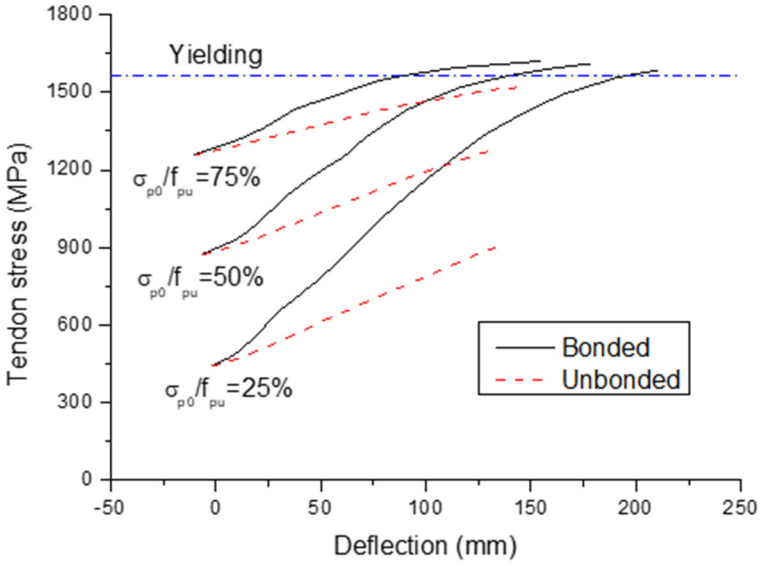


**Figure 10.** Development of tendon stress with the midspan deflection.

Figure 11 presents strain and stress development in nonprestressed steel. The strain development in the beams, except for BPC scenarios having the 25% prestress level, experiences three stages. The transitions are caused by cracking and yielding. The yielding stage is not apparent when bonded tendons with a low prestress level are used. After cracking, the nonprestressed steel strain or stress in UPC beams develops quicker than that that in BPC beams. This can be explained by the fact that at a given post-cracking moment, unbonded tendons develop a lower stress, and hence a larger nonprestressed steel stress is required for section equilibrium, when compared to bonded tendons. According to the material law, once the nonprestressed steel reaches its yield strain of 0.00225, the stress remains constant up to the ultimate. For UPC beams, increasing prestress levels produces smaller ultimate strains in nonprestressed steel, indicating a lower ductility. By contrast, the ultimate nonprestressed steel strains in BPC beams with different prestress levels are almost identical.

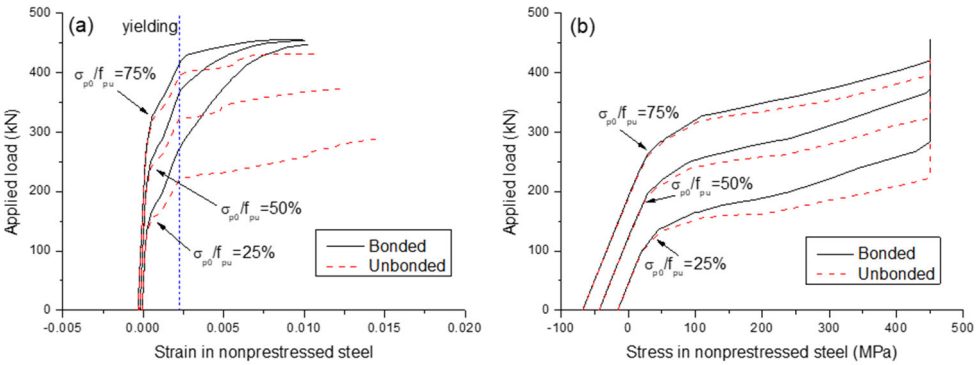


**Figure 11.** Behavior of nonprestressed steel at midspan. (**a**) strain development; (**b**) stress development.

### *3.4. Neutral Axis Depth*

Before introducing the applied load, the whole section is in compression at a 25% prestress level. The concrete strain is around −85 με at the bottom fiber and −25 με at the top fiber, suggesting that the initial neutral axis locates above the top fiber (see Figure 12). At 50% and 75% prestress levels, the bottom fiber is in compression while the top fiber in tension, suggesting that the initial neutral axis lies within the cross section (see Figure 12).

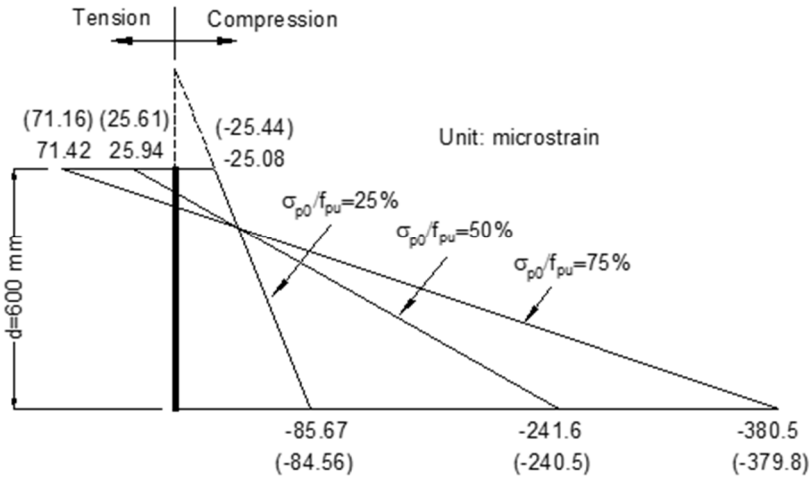


**Figure 12.** Initial concrete strain distribution across section depth at midspan. (BPC beams—data outside the parentheses; UPC beams—data inside the parentheses).

Figure 13a,b illustrate the neutral axis evolutions in the midspan section with the load and curvature, respectively. The neutral axis in UPC beams deviates from that in BPC beams after cracking. The load versus neutral axis depth curves are markedly influenced by the stabilization of crack evolution and the yielding of nonprestressed steel, as illustrated in Figure 13a. At failure, unbonded tendons produce smaller neutral axis depths than bond tendons. Their difference tends to be less notable with the increase of prestress level. Greater prestress levels correspond to higher neutral axis depths in UPC beams, while the effect of prestress level in BPC beams is insignificant.

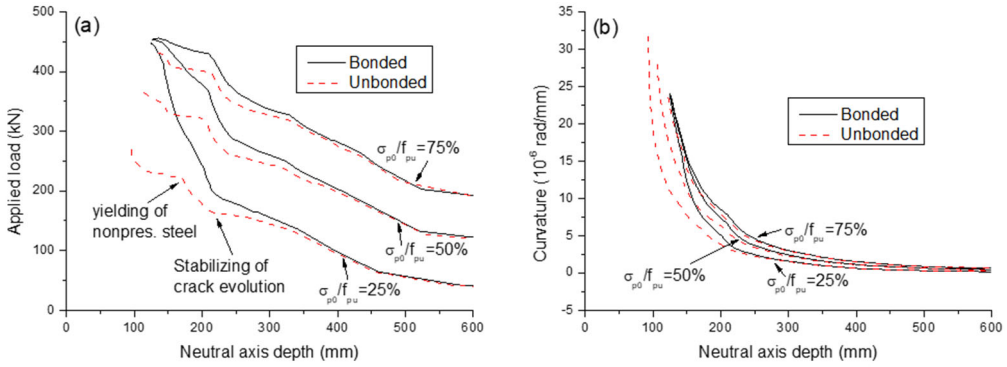


**Figure 13.** Neutral axis evolutions at midspan. (**a**) relationship between applied load and neutral axis depth; (**b**) relationship between curvature and neutral axis depth.

## 4. Moment Redistribution in Continuous Scenarios

Two-span continuous beams having parabolic tendon profile within each span (see Figure 14) are applied for the second stage of study. The tendon eccentricities at end and center supports and midspan are 0, 140 and 140 mm, respectively. The steel areas are: $A_p$ = 450 mm$^2$, $A_{s1}$ = 1440 mm$^2$, $A_{s2}$ = 720 mm$^2$, $A_{s3}$ = 360 mm$^2$, where the subscripts $s1$, $s2$ and $s3$ are nonprestressed tension steels at positive, negative moment regions and nonprestressed compression steel, respectively. Unless otherwise stated, other parameters of the beams are the same as those presented in the previous section.

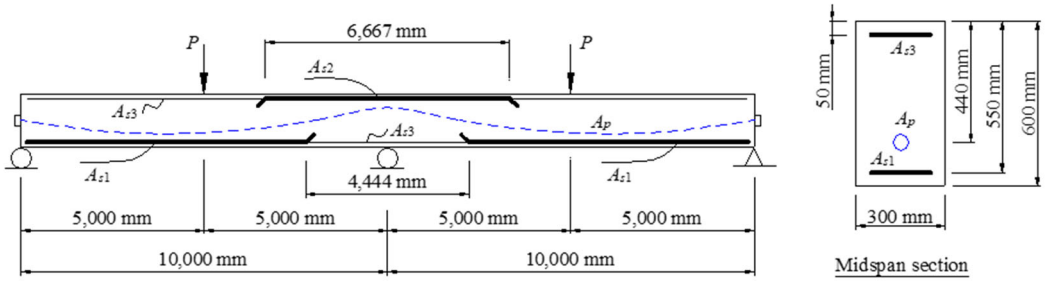


**Figure 14.** Details of continuous PC beams for numerical investigation.

### *4.1. Reaction and Moment*

Figure 15 shows the evolution of end support reactions of both BPC and UPC scenarios having various prestress levels. According the elastic theory, the reaction-load relationship is always linear. The actual reactions obtained by nonlinear analysis deviate from the elastic value when the beams enter into their inelastic range, attributed to the redistribution of support reactions. During the inelastic range of loading, the actual end support reaction is greater than the corresponding elastic value, indicating that the reaction is redistributed from center to end support. The deviation between actual and elastic reactions in UPC beams is more apparent than that of BPC beams and appears to be reduced as the prestress level increases. This observation indicates that higher redistribution is achieved when using unbonded prestressing technique or a lower prestress level.

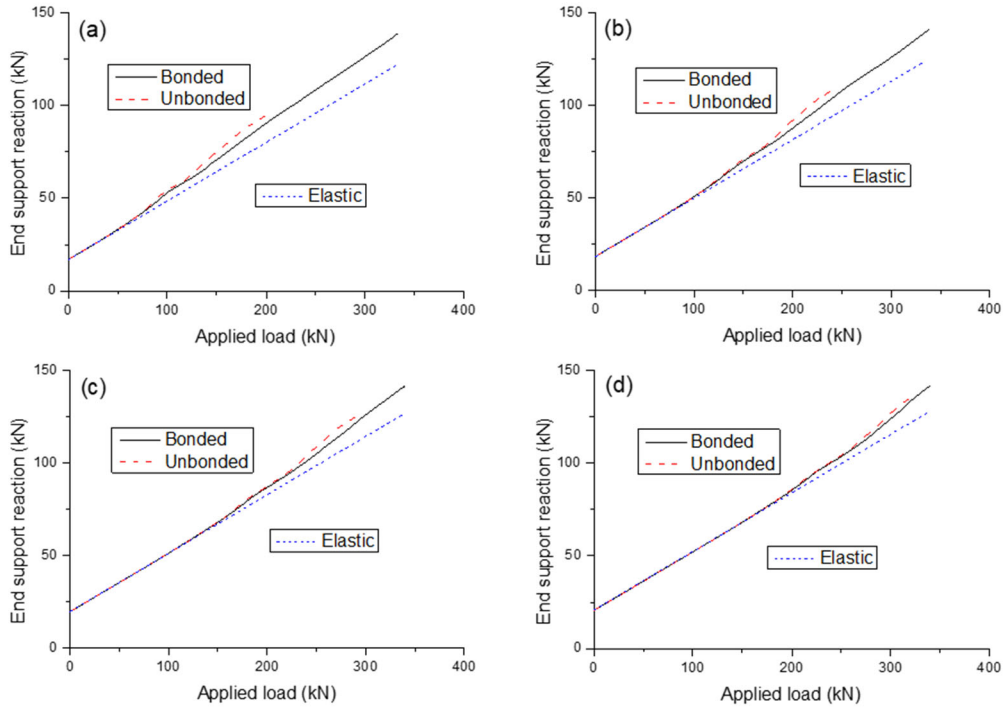


**Figure 15.** Load-reaction curves depending on the prestress level. (**a**) $\sigma_{p0}/f_{pu}$ = 0; (**b**) $\sigma_{p0}/f_{pu}$ = 25%; (**c**) $\sigma_{p0}/f_{pu}$ = 50%; (**d**) $\sigma_{p0}/f_{pu}$ = 75%.

Figure 16 shows the load-moment relationship for BPC and UPC beams with different prestress levels. Different from the elastic moment with a fixed growth rate, the growth of actual moments is impacted by several phases, e.g., the onset of cracking and the formation of plastic hinges. When first cracks appear in center support, its flexural stiffness substantially decreases. Consequently, the moment in the center support is redistributed toward the midspan, leading to a reduction in the growth rate in the center support moment while an increase in the growth rate in the midspan moment. Similar redistribution

behavior is observed on the formation of first plastic hinges. For a given post-cracking load, unbonded tendons commonly lead to higher difference between the actual and elastic moments.

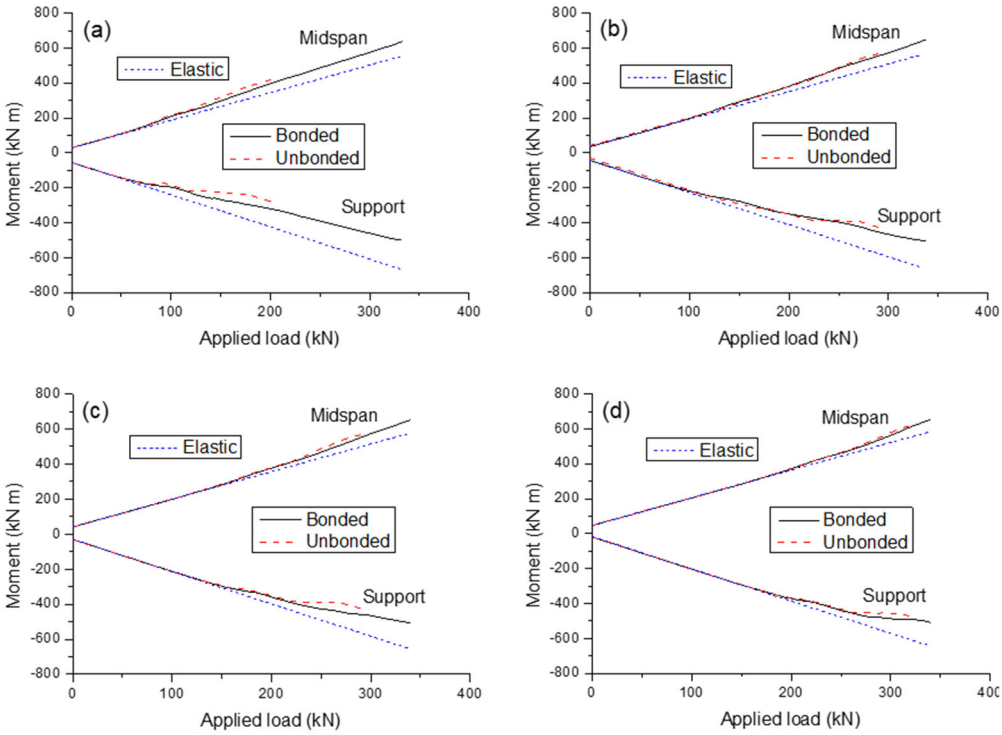


**Figure 16.** Load-moment curves depending on the prestress level. (**a**) $\sigma_{p0}/f_{pu}$ = 0; (**b**) $\sigma_{p0}/f_{pu}$ = 25%; (**c**) $\sigma_{p0}/f_{pu}$ = 50%; (**d**) $\sigma_{p0}/f_{pu}$ = 75%.

Figure 17 demonstrates the evolution of the ratio of the center support moment to the midspan moment (secondary moment and self-weight moment are excluded) in BPC and UPC beams with different prestress levels. Prior to cracking, the moment ratio remains a constant value of 1.17, indicating no redistribution of moments. Beyond cracking, the moment ratio tends to gradually decrease, while the decrease for UPC beams is faster than that for BPC beams. This can be explained by the fact that moments tend to be redistributed away from the center support and that unbonded tendons results in higher moment redistribution than bonded tendons. In addition, the load versus moment ratios curves are typically influenced by several phases including the stabilization of crack evolution, the first yielding and second yielding of nonprestressed steel, as illustrated in Figure 17. This is attributed to that these phases cause marked change in relative stiffness between the midspan and center support sections, which is recognized as the most important factor impacting moment redistribution [17,18].

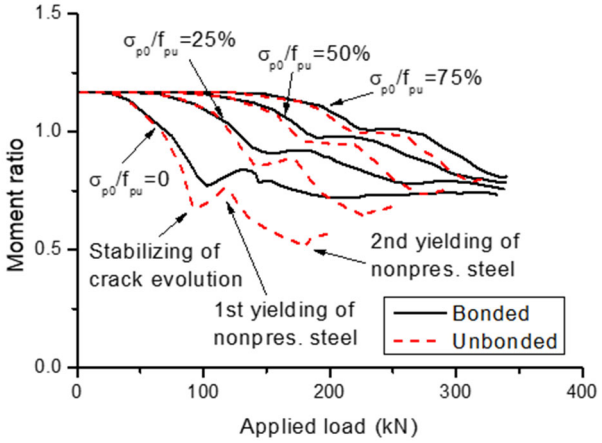


**Figure 17.** Load versus moment ratio curves.

### *4.2. Percentage Moment Redistribution*

Percentage moment redistribution (in failure), $\beta_u$, is expressed by

$$\beta_u(\%) = \frac{M_e - M_u}{M_e} \times 100 \tag{4}$$

where $M_u$ is the ultimate moment and $M_e$ is the elastic moment.

A list of $M_u$, $M_e$ and $\beta_u$ for BPC and UPC beams with various prestress levels is presented in Table 2. Moment redistribution in the beams investigated is positive in the center support and negative in the midspan. The percentage moment redistribution decreases with increasing prestress level. Unbonded tendons produce higher moment redistribution than bonded tendons, notably at a low prestress level. At a zero prestress level, the UPC beam exhibits substantially (around 35%) higher moment redistribution than the BPC beam. The redistribution discrepancy of UPC and BPC scenarios reduces with increasing prestress level, and becomes rather insignificant at the 75% prestress level.

**Table 2.** Values of moments and moment redistribution in continuous beams.

| Bond Condition | Prestress Level | $M_u$ (kN·m) | | $M_e$ (kN·m) | | $\beta_u$ (%) | |
|---|---|---|---|---|---|---|---|
| | | Midspan | Support | Midspan | Support | Midspan | Support |
| Bonded | 0 | 636.8 | −500.5 | 553.3 | −667.4 | −15.1 | 25.0 |
| | 25% | 645.9 | −504.9 | 566.9 | −663.1 | −13.9 | 23.8 |
| | 50% | 649.3 | −508.4 | 576.4 | −654.1 | −12.6 | 22.3 |
| | 75% | 650.7 | −508.2 | 583.6 | −642.4 | −11.5 | 20.9 |
| Unbonded | 0 | 424.5 | −287.2 | 351.9 | −432.4 | −20.6 | 33.6 |
| | 25% | 498.8 | −360.2 | 428.1 | −501.5 | −16.5 | 28.2 |
| | 50% | 569.6 | −430.0 | 501.2 | −566.9 | −13.7 | 24.1 |
| | 75% | 619.0 | −478.8 | 554.1 | −608.6 | −11.7 | 21.3 |

### *4.3. Theoretical Consideration*

The allowable redistribution of continuous RC or PC members suggested in the ACI code [30] is

$$\beta_u(\%) = 1000\varepsilon_t \tag{5}$$

where $\varepsilon_t$ is the net strain in extreme tension steel, suggested greater than 0.0075. The maximum redistribution is 20%.

It is noted that $\varepsilon_t$ is section-dependent and can reflect the flexural ductility of the critical section. However, moment redistribution is member-dependent. Particularly, it is

associated to the relative stiffness of critical sections. In RC continuous beams, the relative stiffness can be symbolized by $\rho_{s2}/\rho_{s1}$, where $\rho_{s1}$ and $\rho_{s2}$ are the tensile reinforcement ratios at the critical positive and negative moment sections, respectively. Lou et al. [17] analyzed the influence of $\rho_{s2}/\rho_{s1}$ in RC continuous beams, and proposed a modified ACI equation by including a parameter $k_s$:

$$\beta_u(\%) = k_s(1000\varepsilon_t) \tag{6}$$

where

$$k_s = 0.68 - 4.21\ln(\rho_{s2}/\rho_{s1}) - 2.05\ln^2(\rho_{s2}/\rho_{s1}) \tag{7}$$

Equation (6) was developed for RC continuous beams. This equation may be extended to be applicable to PC continuous beams by replacing $k_s$ with $k_p$, i.e.,:

$$\beta_u(\%) = k_p(1000\varepsilon_t) \tag{8}$$

where

$$k_p = 0.68 - 4.21\ln(q_2/q_1) - 2.05\ln^2(q_2/q_1) \tag{9}$$

where $q_1$ and $q_2$ are the combined reinforcing indexes at the critical positive and negative moment sections, respectively. The combined reinforcing index $q$ is expressed by

$$q = \begin{cases} \frac{A_p f_{py} + A_s f_y}{b d_p f_{ck}} & \text{for BPC beams} \\ \frac{A_p \sigma_{p0} + A_s f_y}{b d_p f_{ck}} & \text{for UPC beams} \end{cases} \tag{10}$$

where $b$ is the section width; and $d_p$ is the effective tendon depth.

Figure 18a compares the code predictions with FEA results regarding the variation of $\beta_u$ with the prestress level for BPC and UPC beams. According to the ACI code, unbonded tendons lead to a bit lower moment redistribution than bonded tendons. However, this observation is not consistent with FEA predictions, as the latter shows that UPC beams exhibit higher moment redistribution than BPC beams. Therefore, the bond effect cannot be reflected by the ACI code. Moreover, ACI substantially underestimates the moment redistribution, especially in UPC beams having a low prestress level. Figure 18b shows that the predictions of the proposed equation and FEA achieve excellent agreement. In addition, the bond impact on moment redistribution is well reflected by the proposed equation.

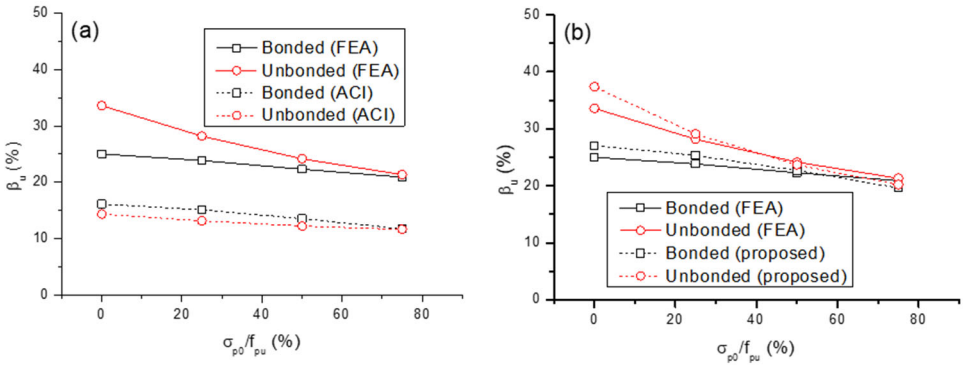


**Figure 18.** Variation of $\beta_u$ with varying prestress level. (**a**) comparison of ACI equation with FEA; (**b**) comparison of proposed equation with FEA.

Figure 19 correlates the redistribution values calculated from the simplified equations to the FEA for the 4 BPC and 4 UPC beams with various prestress levels investigated. It is seen that the ACI code leads to a poor correlation with the FEA. By introducing the parameter $k_p$, the proposed equation predicts very well the moment redistribution in continuous PC scenarios.

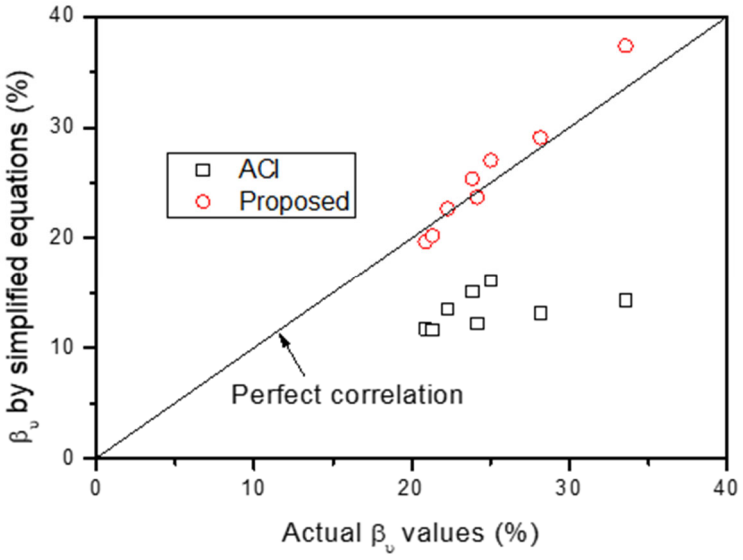


**Figure 19.** Correlation of $\beta_u$ by simplified equations with actual values.

## 5. Conclusions

A two-phase study is performed to investigate the bond effect of steel tendons in PC beams with various prestress levels. In the first phase of study, comprehensive behavior of simply supported PC beams is examined, while in the second phase of study, moment redistribution in continuous PC beams is identified. The main conclusions resulting from the study are:

- Due to the unbonded condition, UPC beams exhibit less favorable crack pattern (i.e., larger crack width with smaller crack zone) than BPC beams. An increase in prestress level could substantially improve the crack pattern of UPC beams.
- The difference between the ultimate loads or deflections of BPC and UPC beams strongly depends on the prestress level, i.e., at 25%, 50% and 75% prestress levels, the ultimate load and deflection of UPC beams are 64.6% and 63.9%, 82.6% and 73.5%, 94.7% and 94.2% of those of BPC beams, respectively.
- The nonprestressed tension steel strain and neutral axis depth (in failure) in BPC beams are independent of the prestress level. By contrast, a greater prestress level produces a smaller nonprestressed tension steel strain but a higher neutral axis depth in UPC beams.
- Unbonded tendons lead to higher moment redistribution (in failure) in continuous PC beams than bonded tendons. The redistribution discrepancy of BPC and UPC beams is substantial at low prestress levels while decreases with increasing prestress level.
- The ACI code cannot well describe the bond impact of steel tendons on moment redistribution. It also significantly underestimates the redistribution value. A modified ACI equation is proposed, and shows good predictions in moment redistribution in both BPC and UPC beams.

It should be noted that the proposed equation for quantifying moment redistribution in continuous BPC and UPC beams is only verified by a limited number of numerical data generated in this study. The reliability and applicability of the proposed equation need to be further validated by extensive experimental data.

**Author Contributions:** Conceptualization, T.L.; Methodology, M.P.; Software, X.L. and Y.D.; Validation, Y.D.; Formal Analysis, M.P.; Investigation, X.L.; Resources, T.L.; Data Curation, X.L. and Y.D.; Writing—Original Draft Preparation, M.P.; Writing—Review and Editing, T.L.; Visualization, M.P.; Supervision, T.L. All authors have read and agreed to the published version of the manuscript.

**Funding:** This research was funded by Portuguese Foundation for Science and Technology, grant number UIDB/00285/2020.

**Institutional Review Board Statement:** Not applicable.

**Informed Consent Statement:** Not applicable.

**Data Availability Statement:** Not applicable.

**Conflicts of Interest:** The authors declare no conflict of interest.

## References


1. Pan, Z.; You, F. Quantitative design of backup prestressing tendons for long-span prestressed concrete box girder bridges. *ASCE J. Bridge Eng.* **2015**, *20*, 04014066. [CrossRef]
2. Lou, T.; Liu, M.; Lopes, S.M.R.; Lopes, A.V. Effect of bond on flexure of concrete beams prestressed with FRP tendons. *Compos. Struct.* **2017**, *173*, 168–176. [CrossRef]
3. Victor, A.J.; Menkulasi, F. A flexural design methodology for composite heterogeneous and homogeneous UHPC bridge beams prestressed with bonded strands. *Eng. Struct.* **2021**, *236*, 112127. [CrossRef]
4. Bonopera, M.; Chang, K.C.; Lin, T.K.; Tullini, N. Influence of prestressing on the behavior of uncracked concrete beams with a parabolic bonded tendon. *Struct. Eng. Mech.* **2021**, *77*, 1–17.
5. Abdelaziz, M.M.; El-Ghazaly, H.A.; Gomaa, M.S. Improved applied element model for bonded prestressed concrete structures. *ASCE J. Struct. Eng.* **2021**, *147*, 04020298. [CrossRef]
6. Choi, J.; Zaborac, J.; Bayrak, O. Assessment of shear capacity of prestressed concrete members with insufficient web reinforcement using AASHTO LRFD general shear design method. *Eng. Struct.* **2021**, *242*, 112530. [CrossRef]
7. Xie, J.; Zhao, X.; Yan, J.B. Experimental and numerical studies on bonded prestressed concrete beams at low temperatures. *Constr. Build. Mater.* **2018**, *188*, 101–118. [CrossRef]
8. Peng, F.; Xue, W. Calculating method for ultimate tendon stress in internally unbonded prestressed concrete members. *ACI Struct. J.* **2019**, *116*, 225–234. [CrossRef]
9. Chang, Z.; Xing, G.; Zhao, J.; Huang, J. Feasibility and flexural behavior of RC beams prestressed with straight unbonded aluminum alloy tendons. *Adv. Struct. Eng.* **2021**, *24*, 1466–1479. [CrossRef]
10. Tang, C.; Zhang, G.; Song, C.; Li, X.; Hou, Y. Flexural Behavior of Unbonded Prestressed Concrete Bridge Girders. *Adv. Civ. Eng.* **2021**, *2021*, 6642513. [CrossRef]
11. Moreira, L.S.; Sousa, J.B.M., Jr.; Parente, E., Jr. Nonlinear finite element simulation of unbonded prestressed concrete beams. *Eng. Struct.* **2018**, *170*, 167–177. [CrossRef]
12. Du, J.S.; Au, F.T.K.; Cheung, Y.K.; Kwan, A.K.H. Ductility analysis of prestressed concrete beams with unbonded tendons. *Eng. Struct.* **2008**, *30*, 13–21. [CrossRef]
13. Hussien, O.F.; Elafandy, T.H.K.; Abdelrahman, A.A.; Abdel Baky, S.A.; Nasr, E.A. Behavior of bonded and unbonded prestressed normal and high strength concrete beams. *HBRC J.* **2012**, *8*, 239–251. [CrossRef]
14. Kodur, V.K.R.; Campbell, T.I. Factors governing redistribution of moment in continuous prestressed concrete beams. *Struct. Eng. Mech.* **1999**, *8*, 119–136. [CrossRef]
15. Lou, T.; Liu, M.; Lopes, S.M.R.; Lopes, A.V. Moment redistribution in two-span prestressed NSC and HSC beams. *Mater. Struct.* **2017**, *50*, 246. [CrossRef]
16. Zhou, W.; Zheng, W.Z. Experimental research on plastic design method and moment redistribution in continuous concrete beams prestressed with unbonded tendons. *Mag. Concr. Res.* **2010**, *62*, 51–64. [CrossRef]
17. Lou, T.; Lopes, S.M.R.; Lopes, A.V. Effect of relative stiffness on moment redistribution in reinforced high-strength concrete beams. *Mag. Concr. Res.* **2017**, *69*, 716–727. [CrossRef]
18. Lou, T.; Peng, C.; Min, D.; Sun, W. Moment redistribution in unbonded prestressed concrete members: Proposed modification of ACI equation. *ACI Struct. J.* **2020**, *117*, 71–80.
19. Lin, T.Y.; Burns, N.H. *Design of Prestressed Concrete Structures*, 3rd ed.; John Wiley & Sons: New York, NY, USA, 1981.
20. Lee, D.H.; Kim, K.S. Flexural strength of prestressed concrete members with unbonded tendons. *Struct. Eng. Mech.* **2011**, *38*, 675–696. [CrossRef]
21. Lou, T.; Lopes, S.M.R.; Lopes, A.V. Numerical modelling of nonlinear behaviour of prestressed concrete continuous beams. *Comput. Concr.* **2015**, *15*, 373–389. [CrossRef]
22. Lou, T.; Lopes, S.M.R.; Lopes, A.V. Nonlinear and time-dependent analysis of continuous unbonded prestressed concrete beams. *Comput. Struct.* **2013**, *119*, 166–176. [CrossRef]
23. Zheng, W.Z.; Wang, X.D. Ultimate stress increase in unbonded tendons in prestressed concrete beams. *J. Zhejiang Univ. SCIENCE A* **2010**, *11*, 998–1014. [CrossRef]
24. Halder, R.; Yuen, T.Y.P.; Chen, W.W.; Zhou, X.; Deb, T.; Zhang, H.; Wen, T.H. Tendon stress evaluation of unbonded post-tensioned concrete segmental bridges with two-variable response surfaces. *Eng. Struct.* **2021**, *245*, 112984. [CrossRef]
25. Yuen, T.Y.P.; Halder, R.; Chen, W.W.; Zhou, X.; Deb, T.; Liu, Y.; Tseng, Y.; Wen, T.H. DFEM of a post-tensioned precast concrete segmental bridge with unbonded external tendons subjected to prestress changes. *Structures* **2020**, *28*, 1322–1337. [CrossRef]
26. Bonopera, M.; Chang, K.C.; Chen, C.C.; Sung, Y.C.; Tullini, N. Feasibility study of prestress force prediction for concrete beams using second-order deflections. *Int. J. Struct. Stab. Dyn.* **2018**, *18*, 1850124. [CrossRef]

27. *EN 1992-1-1*; Eurocode 2 (EC2): Design of Concrete Structures—Part 1-1: General Rules and Rules for Buildings. European Committee for Standardization: Brussels, Belgium, 2004.
28. Menegotto, M.; Pinto, P.E. *Method of Analysis for Cyclically Loaded Reinforced Concrete Plane Frames*; IABSE Preliminary Report for Symposium on Resistance and Ultimate Deformability of Structures Acted on Well-Defined Repeated Loads; IABSE: Lisbon, Portugal, 1973; pp. 15–22.
29. Du, G.; Tao, X. Ultimate stress of unbonded tendons in partially prestressed concrete beams. *PCI J.* **1985**, *30*, 72–91.
30. *ACI Committee 318*; Building Code Requirements for Structural Concrete (ACI 318-11) and Commentary. American Concrete Institute: Farmington Hills, MI, USA, 2011.